JOC The Journal of Organic Chemistry

Article

pubs.acs.org/joc

Theoretical Investigations toward the [4 + 2] Cycloaddition of Ketenes with *N*-Benzoyldiazenes Catalyzed by N-Heterocyclic Carbenes: Mechanism and Enantioselectivity

Wenjing Zhang, Yanyan Zhu,* Donghui Wei, Yunxia Li, and Mingsheng Tang*

The College of Chemistry and Molecular Engineering, Zhengzhou University, Zhengzhou, Henan Province 450001, P. R. China

Supporting Information

ABSTRACT: Density functional theory (DFT) calculations have been performed to provide the first detailed computational study on the mechanism and enantioselectivity for the [4 + 2] cycloaddition reaction of ketenes with *N*-benzoyldiazenes catalyzed by N-heterocyclic carbenes (NHCs). Two possible mechanisms have been studied: first is the "ketene-first" mechanism (mechanism A), and second is the novel "diazene-first" mechanism (mechanism B). The calculated results reveal that mechanism B is more favorable than mechanism A because it is not only of lower energy barrier but also more consistent with the provided general experimental procedure (Huang, X.-L.; He, L.; Shao, P.-L.; Ye, S. *Angew. Chem., Int. Ed.* **2009**, *48*, 192−195). The enantioselectivity-determining step is demonstrated to present during the first process of cycloaddition, and the main product configuration is verified to agree with the experimental ee values very well. This study should be of some worth on forecasting how different substituent groups of catalysts and/or reactants affect the enantioselectivity of products. The obtained novel mechanistic insights should be valuable for not only rational design of more efficient NHC catalysts but also understanding the general reaction mechanism of [4 + 2] cycloaddition of ketenes.

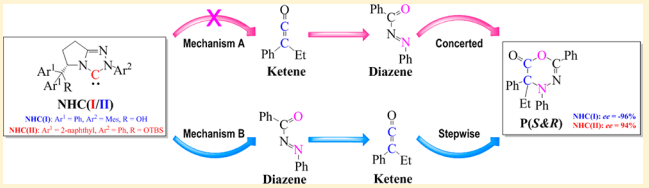

1. INTRODUCTION

Since it was first introduced by Staudinger around a century ago, the cycloaddition of ketenes has been one of the most useful and effective approaches to heterocyclic compounds.[1] For a long time, applications of N-heterocyclic carbenes (NHCs) in organocatalysis have drawn a great deal of interest because of its numerous attractive properties,[2] including pronounced nucleophilicity,[3] good potential of being leaving group,[4] and tunable electronic and steric properties by choosing different nitrogen heterocycles and/or the substituents on the 1- and 3- position.[3,5] One of the most well-known applications of NHCs as the organocatalyst is in umpolung reactions such as the benzoin condensation[6] or the Stetter reaction.[7] In particular, Ye and co-workers have exerted much efforts toward the NHC catalytic cycloaddition of ketenes, such as [2 + 2] ketene/imine,[8] ketene/aldehyde,[9] [2 + 2 + 2] ketene/carbon disulfide,[10] and [4 + 2] ketene/enone.[11]

Recently, Ye reported a highly enantioselective [4 + 2] cycloaddition of ketenes **1** with *N*-benzoyldiazenes **2** catalyzed by chiral NHCs (**NHC(I/II)**) to give 1,3,4-oxadiazin-6-ones **P**(***R*** and ***S***) (Scheme 1).[12,13] In addition to its potential biological activity,[14] this highly functionalized lactone is also a useful intermediate in organic synthesis.[15] For example, it can be regarded as the masked α, α-disubstituted amino acid derivative.[16] What is more interesting, they discovered that when catalyst **NHC(I)** was replaced by **NHC(II)**, the reaction enantioselectivity would be completely switched from a preferred *S* configuration (−96% ee) to a preferred *R* configuration (94% ee).

In contrast to those successful practical applications, synchronous theoretical investigations about NHC-catalyzed cycloadditions have been quite limited, except for some DFT study efforts on the [2 + 2] reaction of ketene. For example, Liu and co-workers[17] have exerted investigations toward the Staudinger reaction ([2 + 2] cycloaddition of a ketene with an imine) and found that the "ketene-first" mechanism is exclusively more favorable to the "imine-first" catalytic cycle. Moreover, Liu also revealed that a different nitrogen substituent on the imine would cause the NHC-catalyzed Staudinger reaction to exhibit different stereoselectivities. Our previous DFT study[18] has elucidated a possible mechanism for the enantioselective synthesis of aza-β-lactams via NHC-catalyzed [2 + 2] cycloaddition of ketene with diazenedicarboxylate (Scheme 2), in which the frontier molecular orbital (FMO) and global reactivity indexes (GRI)[19] analyses were performed to illustrate why NHC catalyst could make the reaction occur more easily.

Nevertheless, to the best of our knowledge, there has been no detailed mechanistic investigation on the NHC-catalyzed [4 + 2] cycloadditions of ketene, and the catalytic cycle remains unclear. It is known that the asymmetric aza-[4 + 2] cycloaddition of a conjugated diazene with a substituted alkene is among the most powerful available methodologies for the preparation of optically active nitrogen-containing compounds,[20,21] which are the key building blocks for the construction of valuable compounds such as amino acids, aza

Received: September 22, 2012
Published: November 15, 2012

Scheme 1. Title Catalytic Reaction

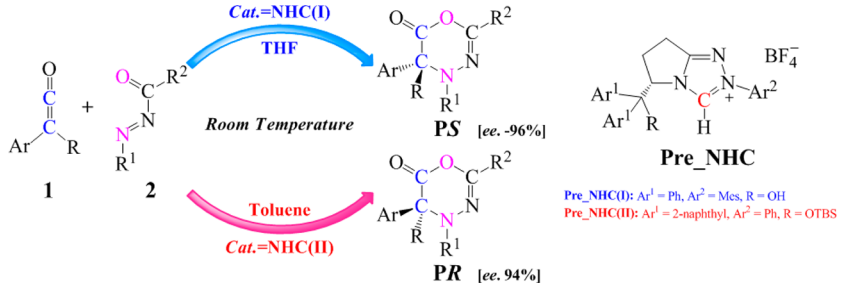

Scheme 2. [2 + 2] Cycloaddition Studied in Our Previous Work[18]

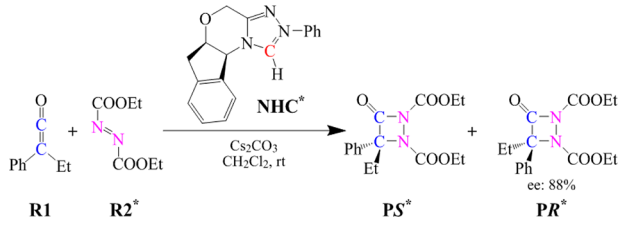

sugars, and alkaloids. Therefore, it is of significant importance to perform a theoretical study toward this NHC-catalyzed aza-[4 + 2] cycloaddition in terms of obtaining more details at the molecular level and understanding its mechanism thoroughly.

In regard to the title reaction displayed in Scheme 1, a possible reaction mechanism has been proposed[12] (Scheme 3).

Scheme 3. Possible Catalytic Cycle Supposed by Ye

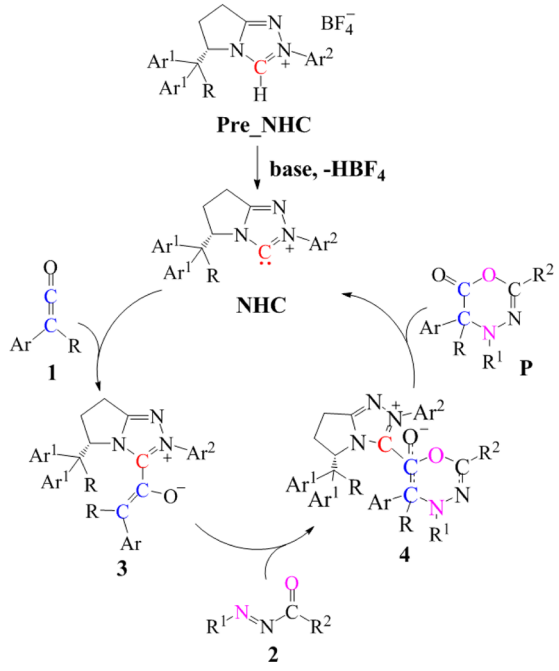

It suggests that the catalytic cycle is initiated by nucleophilic addition of **NHC** to ketene **1** to give the triazolium enolate **3**, which subsequently reacts with the diazene **2** by a synergetic [4 + 2] cycloaddition to give the adduct **4**. Final elimination of **NHC** furnishes the corresponding 1,3,4-oxadiazin-6-one **P** and regenerates the catalyst. However, this plausible mechanism is contradictory to their general experimental procedure,[22] which states that the diazene **2** is added to the heterogeneous mixture of trazolium salt, Cs_2CO_3, and solvent prior to the other reactant ketene **1**. In particular, a colored solution appeared after the diazene addition, and the following ketene addition led the system to become transparent again. This special addition sequence of the two reactants and the special colored solution inspired us to imagine that it the combination of diazene **2** with NHC should initiate the reaction and the colored compound be broken by its reaction with the ketene **1**. Is this presumption the truth? What is the exact reason for the colored solution? Challenges to elucidate a reliable mechanism that is consistent with the experimental results and to provide a reasonable explanation for the catalyst-dependent enantioselectivity motivate our present work.

2. COMPUTATIONAL DETAILS

All theoretical calculations were performed using the Gaussian 09 program,[23] with the density functional theory (DFT) that has been widely utilized in the study of reaction mechanisms.[24] Our previous study[18] indicated that the B3LYP functional calculations account well for the experimental results regarding the NHC-catalyzed cycloadditions of ketene. The B3LYP functional was thus selected to carry the DFT calculations (for our reasons for ruling out the M05-2X functional, see the Supporting Information). All structures of the reactants, products, transition states, and intermediates were optimized and characterized as minima or transition states at the B3LYP/6-31G* level in the gas phase at 298.15 K and 1 atm. The same level of intrinsic reaction coordinate (IRC) calculations[25,26] were performed to ensure that the transition states led to the expected reactants and products. Based on the optimized structures, the energies were then refined by the B3LYP/6-311+G** single-point calculations with the solvent effects included (toluene for **NHC(I)**-catalyzed system and THF for **NHC(II)**-catalyzed system, which were chosen from the available experiment[12]) and simulated by IEFPCM[27] model. All energies reported in this paper include the zero-point vibrational energy (ZPVE) corrections obtained from the frequency calculations at the B3LYP/6-31G* level in the gas phase. Natural bond orbital (NBO)[28] analyses were performed with the same basis set to assign the atomic charges (Q). The suitability of single-point energy refinements based on the structures optimized using the relatively small 6-31G* basis set was examined (see Table S2, Supporting Information).[29] We selected some stationary points and fully optimized them at the B3LYP/6-311+G** level with solvent effects included. The relative energetic results from these optimization calculations agree with the refined values within a deviation of <0.6 kcal/mol. The TDDFT (time-dependent DFT) calculations were

dx.doi.org/10.1021/jo302044n | J. Org. Chem. 2012, 77, 10729−10737

Scheme 4. Two Proposed Mechanisms for the Title Reaction: "Ketene-First" Mechanism A (Left Cycle) and the "Diazene-First" Mechanism B (Right Cycle)

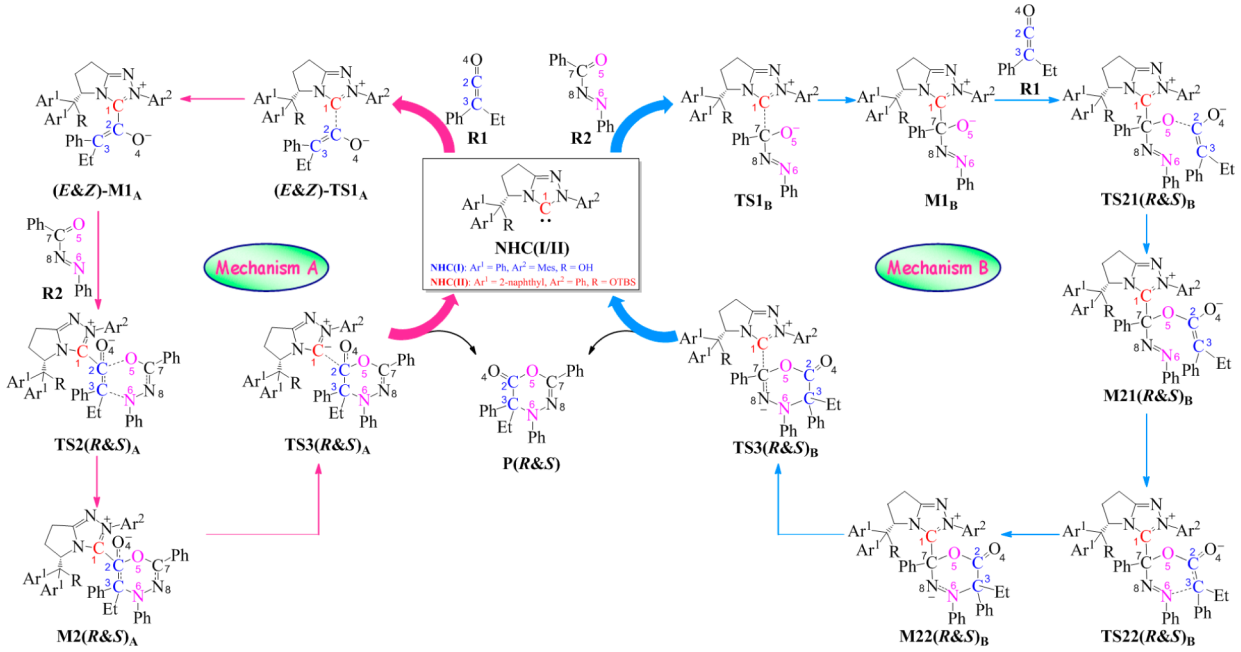

carried out at the B3LYP/6-31G* level based on the optimized ground-state geometries in gas phase.

3. RESULTS AND DISCUSSION

All computational models were selected on the basis of the experimental results.[12] We chose the substituent groups Ar = Ph, R = Et, and R^1 = R^2 = Ph because they construct the simplest reactant structures and also afford relatively high yields and ee values. That is, as shown in Scheme 4, the compounds of phenyl ethyl ketene (denoted as **R1**) and *N*-benzoyl-*N*′-phenyldiazene (denoted as **R2**) were chosen as the object of investigation.

3.1. Optimization of the Two Catalysts. In advance of all discussions, an examination about the accuracy of our computational methods to structure optimization has been conducted. Figure 1 provides the superposition results of the optimized structures (yellow) with the X-ray crystallographic structures (purple) of the two catalysts. What is noteworthy is that both the experimental structures are picked from the corresponding precursors of NHCs with cutting a molecular of

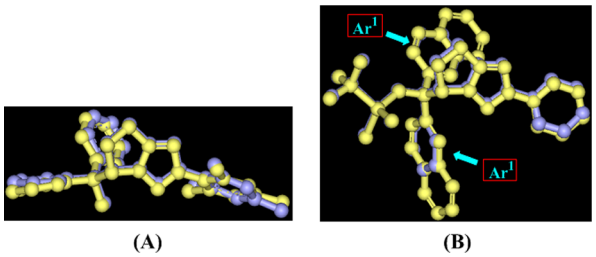

Figure 1. Superposition of the optimized structures (yellow) with X-ray crystallographic structures (purple) for the two catalysts: (A) **NHC(I)** (structure in purple was chosen from the X-ray crystallographic structure of the **NHC(I)** precursor with a cutaway of the HBF_4 molecule); (B) **NHC(II)** (structure in purple was chosen from the X-ray crystallographic structure of **NHC(II′)** precursor with a cutaway of the HBF_4 molecule). All hydrogen atoms are omitted.

HBF_4. Since the crystal structure of **NHC(II)** is unavailable from the experimental results,[12] we used **NHC(II′)** to replace it in which the substituent groups Ar^1 = Ph instead of Ar^1 = 2-naphthyl in **NHC(II)**. Obviously, the calculated and experimental structures overlap with each other very well. Therefore, we can conclude that the computational methods and levels used in the present work are reasonable and reliable to structure optimization.

3.2. Reaction Mechanism. On the basis of their characteristics, it is reasonable to predict that the reaction mechanisms of **NHC(I)**-catalyzed system and **NHC(II)**-catalyzed system should be quite similar. Thus, we have only performed detailed calculations on the reaction with **NHC(I)** as catalyst. The detailed processes of "ketene-first" mechanism A (left cycle) and the "diazene-first" mechanism B (right cycle) are illustrated in Scheme 4. Figures 2 and 4 display all of the optimized structures involved in mechanisms A and B, respectively. The calculated energy profiles are presented in Figure 3, and the free energy profiles are shown in the Supporting Information (Figure S2). It is necessary to emphasize that the entropic penalty in thermal corrections based on the ideal gas phase model are often overestimated because the suppressing effects of the solvent and pressure on the translational and rotational degrees of freedom of the reactants can not be properly accounted for by the gas phase model. Unless otherwise specified, the energies of **NHC(I)** + **R1** + **R2** are set as 0.0 kcal/mol as reference.

3.2.1. Mechanism A. As we can see from Scheme 4, there are three steps involved in mechanism A, including the nucleophilic attack of catalyst **NHC(I)** to the ketene **R1**, the concerted [4 + 2] cycloaddition process, and finally the release of target products **P(*R*/*S*)** accompanied by recovery of catalyst.

In the first step, the *exo* and *endo* attacks of carbene atom C1 in **NHC(I)** to the atom of C2 in **R1** give $\mathbf{M1_A}$ in *E* and *Z* configurations (denoted as **(*E*/*Z*)-M1$_A$**) via transition states **(*E*/*Z*)-TS1$_A$**, respectively. As shown in Figure 2, the distance between the C1 and C2 atoms is shortened from 2.52 Å in ***E***-

dx.doi.org/10.1021/jo302044n | J. Org. Chem. 2012, 77, 10729−10737

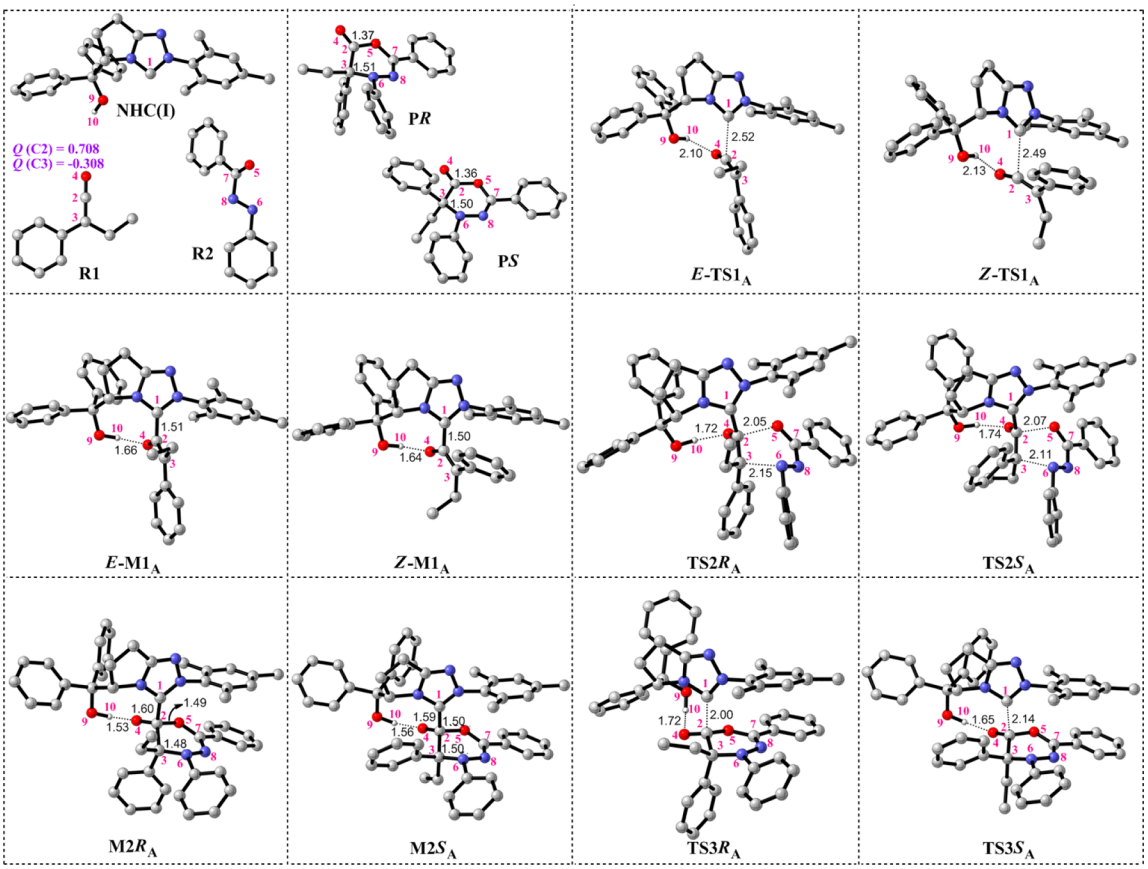

Figure 2. Optimized geometries of all the stationary points involved in mechanism A (hydrogen atoms not involved in reaction sites are omitted; bond lengths in angstroms; NBO charges (Q) in e).

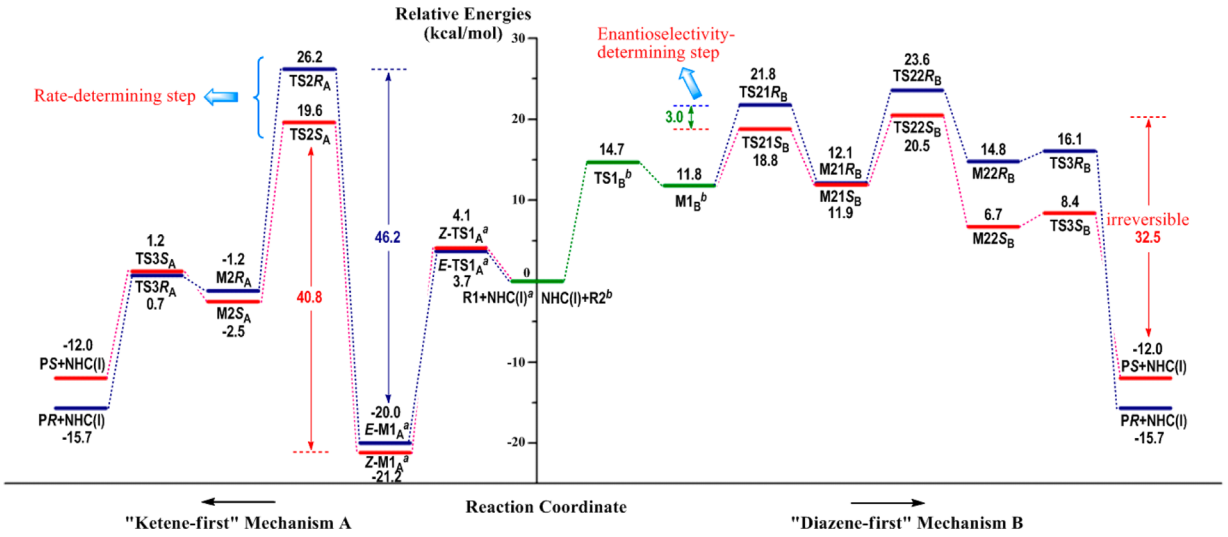

Figure 3. Energy profiles of mechanism A (left) and mechanism B (right) (units in kcal/mol for energies; the superscripts *a*, *b* represent adding energies of **R2**, **R1**, respectively).

TS1$_A$ and 2.49 Å in ***Z*-TS1**$_A$ to 1.51 Å in ***E*-M1**$_A$ and 1.50 Å in ***Z*-M1**$_A$, respectively, which indicates the full formation of the C1−C2 bond. In addition, as displayed in the energy profiles in Figure 3, the energy barriers of the *exo* and *endo* attack processes are 3.7 and 4.1 kcal/mol, respectively. This difference is so slight that it may not be sufficient to determine the reaction enantioselectivity. The addition products ***E*-M1**$_A$ and ***Z*-M1**$_A$ are 20.0 and 21.2 kcal/mol more stable than the initial reactants, which may be partially attributed to the formed hydrogen bonds O9−H10···O4, with distances between H10 and O4 1.66 Å in the *E* configuration and 1.64 Å in the *Z* configuration, respectively.

During the subsequent step, four possible reaction patterns can be involved (Table 1): for both the *exo* or *endo* attack product (*E*/*Z*)-**M1**$_A$, the second reactant **R2** can take either the *Re* or *Si* face to participate in the [4 + 2] cycloaddition process.

dx.doi.org/10.1021/jo302044n | J. Org. Chem. 2012, 77, 10729−10737

Table 1. Four Possible Reaction Patterns for the Second Step of Mechanism A

reaction pattern	configuration of $\mathbf{M1}_A$	addition face of **R2**	product
R_{exo}	*E*	*Re*	**PR**
R_{endo}	*Z*	*Re*	**PS**
S_{exo}	*E*	*Si*	**PS**
S_{endo}	*Z*	*Si*	**PR**

However, taking steric effects derived from the hydrogen bond O9−H10···O4 into consideration, we only considered the reaction occurring at the less-hindered *Re* face (R_{exo} and R_{endo}).

The IRC computational results have demonstrated that the two transition states ($\mathbf{TS2}(R/S)_A$) present in this step absolutely lead to the expected reactants and products. Therefore, we can conclude that this cycloaddition reaction belongs to the concerted fashion.

The energy barriers for the second step via $\mathbf{TS2}R_A$ or $\mathbf{TS2}S_A$ are 46.2 and 40.8 kcal/mol, respectively (Figure 3).[30] This energy difference indicates the consistent enantioselectivity with the experimental results (*S* configuration favorable),[12] but they are obviously too high for the reaction to occur at room temperature. Moreover, the marked endothermic property of this step has further demonstrated the infeasibility of mechanism A.

In the last step of mechanism A, the very low energy barriers via transition states $\mathbf{TS3}R_A$ and $\mathbf{TS3}S_A$ (1.9 and 3.7 kcal/mol, respectively, shown in Figure 3) indicate that it is easy for the catalyst **NHC(I)** to be recycled, which corroborates its potential as a good leaving group.[2,4]

3.2.2. Mechanism B. As shown in Scheme 4, mechanism B follows the assumption that it should be the reactant **R2** that combines with the catalyst in advance. As a result, the [4 + 2] cycloaddition process changes to occur through the step-by-step mechanism based on our computational research. The detailed calculated results are illustrated as follows:

There are four steps involved in mechanism B, including the nucleophilic attack of **NHC(I)** to **R2**, then the two stepwise bonding processes of C2 atom with O5 atom and C3 atom with N6 atom, and finally release of the products and catalyst.

Scheme 5 illustrates stereochemistry of the nucleophilic addition step. It is clear that the catalyst **NHC(I)** can attack **R2** from either the *Re* or *Si* face. However, in order to avoid hindrance to the approach of **R1** in the next step, the reactive atoms O5 and N6 must remain opposite the hydroxyl. That is, the N8═N6 bond and the N6-phenyl group in **R2** will stretch to the back of the triazole (look from the vertical direction of paper in Scheme 5) when attack occurs at the *Si* face. As can be seen from their optimized structures shown in Figure 2, one of the phenyl groups of **NHC(I)** is located at the back of the triazole, which together with the back methyl of the mesitylene, will lead to more serious steric hindrance toward the double bond N8═N6 and the N6-phenyl group in **R2** from the *Si* face than to the phenyl group from the *Re* face. Thus, we only considered the reaction from the less hindered *Re* face.

Scheme 5. Illustration of the Stereochemistry in the First Step of Mechanism B

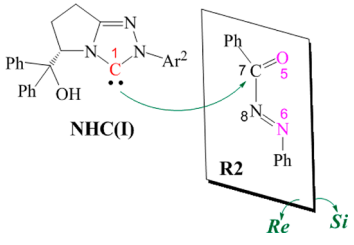

As displayed in Figure 4, with the approach of **NHC(I)** to **R2**, the distance between C1 and C7 is shortened from 1.78 Å in transition state $\mathbf{TS1}_B$ to 1.66 Å in intermediate $\mathbf{M1}_B$. The energy barrier of this step is 14.7 kcal/mol (right half of Figure 3), which is easily crossed under the experimental conditions.[12] This step of the reaction is also demonstrated to be an endothermic reaction as $\mathbf{M1}_B$ lies 11.8 kcal/mol higher than the reactants.

The following two steps are the stepwise [4 + 2] cycloaddition reactions, including the successive C2−O5 bond formation and C3−N6 bond formation. In order to confirm which step proceeds first, we checked the NBO charges distributed on the four atoms (shown in purple beside the relative optimized structures in Figures 2 and 4). Obviously, the positive charge on the C2 atom of **R1** (Q = 0.708 *e*) and the negative value on the O5 atom of $\mathbf{M1}_B$ (Q = −0.771 *e*) indicates the facility for the C2 atom to combine with the O5 atom, while the both negative charges populated on C3 and N6 atoms demonstrate the impossibility of C3−N6 bond formation in the first step.

Similar to the nucleophilic attack of **NHC(I)** to **R1** presented in mechanism A, the first process of cycloaddition here is initiated by $\mathbf{M1}_B$ attacking **R1** in either the *endo* or *exo* pattern through the corresponding transition state $\mathbf{TS21}R_B$ or $\mathbf{TS21}S_B$, which leads to the complexes in the *R* or *S* configuration ($\mathbf{M21}(R/S)_B$), respectively (Figure 4). The bond length of C2−O5 is shortened from 1.93 Å in $\mathbf{TS21}R_B$ to1.46 Å in $\mathbf{M21}R_B$, and 1.94 Å in $\mathbf{TS21}S_B$ to 1.47 Å in $\mathbf{M21}S_B$, respectively, which indicates fully formation of the C2−O5 bond. The energy of $\mathbf{TS21}R_B$ is 3.0 kcal/mol higher than that of $\mathbf{TS21}S_B$, which is mainly due to the different steric effect derived from different approach orientation with **R1** gradually close to $\mathbf{M1}_B$. For example, the steric repulsion of the N6-phenyl group in $\mathbf{M1}_B$ against the phenyl of **R1** may construct one of the possible reasons which lead to the *R* configuration less energetically favorable. Noteworthy, the newly formed hydrogen bond O9−H10···N8 in $\mathbf{TS21}(R/S)_B$ and all the following stationary points involved in Mechanism B (shown in Figure 4) helps to stabilize the corresponding structures.

The second process of cycloaddition involves the bonding reaction between C3 atom and N6 atom. The gradually distance shortening between these two atoms (from 3.16 and 2.87 Å in $\mathbf{M21}(R/S)_B$ to 2.06 and 2.09 Å in $\mathbf{TS22}(R/S)_B$, and finally 1.54 and 1.53 Å in $\mathbf{M22}(R/S)_B$, respectively, as shown in Figure 4) has definitely confirmed the bond formation process in the *R* and *S* reaction pattern. The difference of energy barrier between *R* and *S* configuration transition state is 2.9 kcal/mol, which further demonstrates the more favorable character of the reaction via $\mathbf{TS22}S_B$. As depicted in the energy profiles in Figure 3, the newly formed intermediate of *S* configuration ($\mathbf{M22}S_B$) is significantly more stable than its enantiomer $\mathbf{M22}R_B$, which we believe should be mainly attributed to the different interactions between one of the phenyl groups from **NHC(I)** and the N6-phenyl substituent from **R2** moiety. As illustrated in Figure 4, they are in twisted conformation in $\mathbf{M22}R_B$, whereas a $\pi-\pi$ stacking presents in $\mathbf{M22}S_B$.

In the last step of mechanism B, the catalyst **NHC(I)** is released with the C1−C7 bond broken, the change in whose

dx.doi.org/10.1021/jo302044n | J. Org. Chem. 2012, 77, 10729−10737

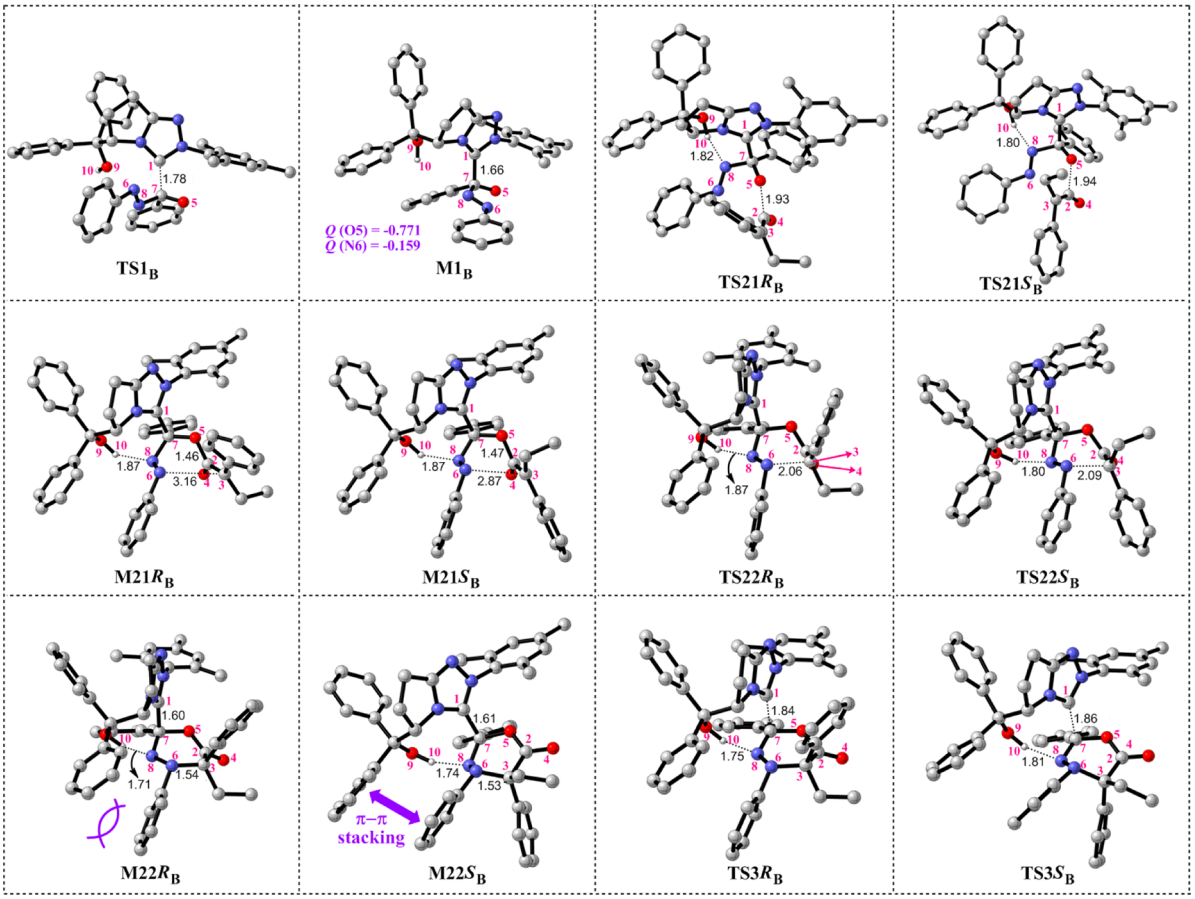

Figure 4. Optimized geometries of all the stationary points involved in mechanism B (hydrogen atoms not involved in reaction sites are omitted; bond lengths in angstroms; NBO charges (Q) in e).

bond length reflects the nature of this reaction process. As shown in Figure 4, the C1−C7 is elongated from 1.60 and 1.61 Å in **M22**$(R/S)_B$ to 1.84 and 1.86 Å in **TS3**$(R/S)_B$, respectively. The energy barrier of this elementary step is 1.3 and 1.7 kcal/mol via **TS3**$(R/S)_B$, respectively, which means **NHC(I)** is easy to be released from the products **P**$(R/S)_B$ and thus, enter the catalytic cycle again.

Taking both mechanisms discussed above into consideration, the energy barrier of mechanism A is 46.2 and 40.8 kcal/mol for the rate-determining step via **TS2**$(R/S)_A$, while it is 23.6 and 20.5 kcal/mol for mechanism B via **TS22**$(R/S)_B$. We can easily conclude that mechanism B is more energetically favorable. In addition, as shown in Figure 3, the first process of [4 + 2] cycloaddition via **TS21**$(R/S)_B$ should apparently be the enantioselectivity-determining step in Mechanism B, which implies the coincident preferred configuration (S) with experimental results[12] for the **NHC(I)**-catalyzed system.

Moreover, as stated above about the general experimental procedure, reactant **R2** is first added to the catalytic reaction system, accompanied with affording of a colored solution, and then the mixed solution of **R1** with solvent is added, leading to the system return to be colorless. As we all know, a typical human eye will respond to wavelengths from about 380 to 750 nm, which corresponds to an electronic transition energy band in the vicinity of 3.27 to 1.65 eV.[31] Here we performed the TDDFT (time-dependent DFT) calculations to some key stationary points in order to obtain their excitation energies. All results were displayed in Table 2. As can be seen, only energies of the three intermediates, (E/Z)-**M1**$_A$ and **M1**$_B$, fall into the visible spectrum area. However, (E/Z)-**M1**$_A$ cannot account for the colored solution because **R1** has not been added to the reaction system when this phenomenon appears. Thus, we consider this color change process should be due to generation of the intermediate **M1**$_B$. That is to say, when **R2** is added, the generation of **M1**$_B$ leads to the colored solution. While after **R1** involved, **M1**$_B$ reacts with **R1** and finally forms the colorless products **P**(R/S). This conclusion further confirms the rationality and feasibility of "diazene-first" mechanism B.

Table 2. TDDFT Computational Results of Some Stationary Points at B3LYP/6-31G* level, Based on the Optimized Ground-State Geometries

	excitation energy[a] (eV)	f[b]	composition[c]	CI[d]
NHC(I)	5.12	0.0095	HOMO-1 → LUMO	0.63463
R1	4.73	0.0279	HOMO → LUMO+1	0.35646
			HOMO → LUMO+2	0.55659
R2	3.63	0.0423	HOMO-5 → LUMO	0.47286
			HOMO-1 → LUMO	0.41114
***E*-M1**$_A$	2.58	0.0237	HOMO → LUMO	0.68829
***Z*-M1**$_A$	2.70	0.0242	HOMO → LUMO	0.69260
M1$_B$	2.71	0.0207	HOMO-1 → LUMO	0.69170
PR	3.87	0.2641	HOMO → LUMO	0.68595
PS	3.62	0.3154	HOMO → LUMO	0.68346

[a]Only the selected low-lying excited states are presented. [b]The oscillator strengths. [c]Only the main configurations are presented. [d]The CI coefficients are in absolute values.

dx.doi.org/10.1021/jo302044n | J. Org. Chem. 2012, 77, 10729−10737

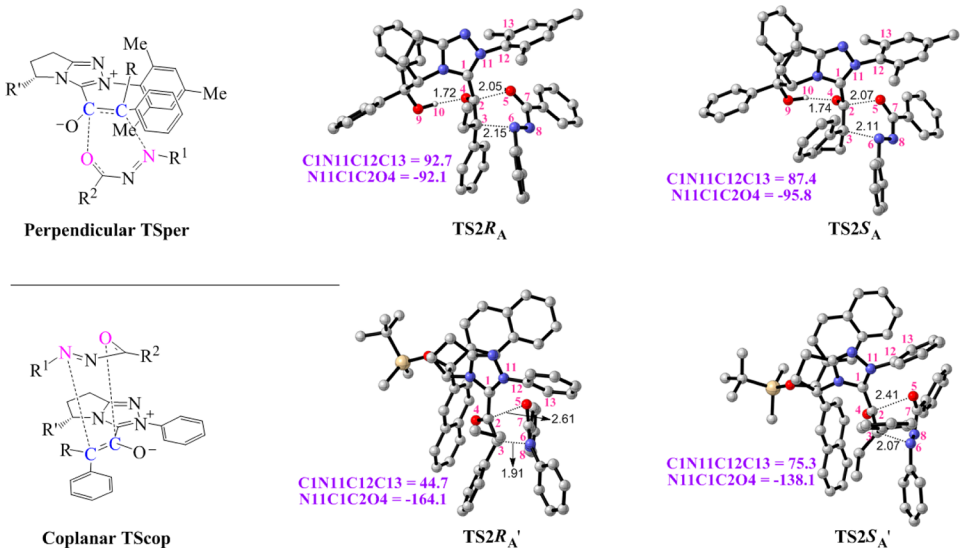

Figure 5. Comparisons of the transition-state structures proposed by Ye (**TSper** and **TScop**) with those calculated in this study at the B3LYP/6-31G* level (bond lengths in angstroms, dihedral angles in degrees).

3.3. Reaction Enantioselectivity. *3.3.1. Explanation by Ye's group.* In an attempt to explain the opposite enantioselectivities catalyzed by **NHC(I)** and **NHC(II)**, Ye and co-workers proposed two possible transition state structures on the basis of their X-ray structural difference (Figure 5). In **TSper**, the *N*-mesityl group of **NHC(I)**, the triazole, and the enloate are perpendicular, while in **TScop**, the *N*-phenyl group of **NHC(II)**, the triazole, and the enloate are coplanar. They believe the perpendicular **TSper** is favored when the reaction is catalyzed by **NHC(I)**, which will give the cycloaddition product of *S* configuration as the major enantiomer, while the coplanar **TScop** is favored when the reaction is catalyzed by **NHC(II)**, which will lead to the product of *R* configuration as the major enantiomer.

Actually, according to the optimized structures of **TS2**(R/S)$_A$ (Figure 5), the dihedral angles of C1N11C12C13 and N11C1C2O4 clearly correspond to the perpendicular conformation depicted in **TSper**. For the **NHC(II)**-catalyzed system, however, only one of the four dihedral angles (N11C1C2O4 in **TS2**R_A′) indicates the approximately coplanar conformation of the triazole toward enloate moiety. The other three related angles deviate from both the perpendicular and coplanar structures. This proposition is of limited value to help understand the reaction enantioselectivity since it is based on an unreliable mechanism, the "ketene-first" mechanism A.

3.3.2. Enantioselectivity-Determining Step. On the basis of conclusions obtained in previous section, in "diazene-first" mechanism B, the enantioselectivity-determining step presents in the reaction process via **TS21**(R/S)$_B$, and it indicates the same preferred configuration (*S*) with experimental results[12] for the **NHC(I)**-catalyzed system.

In regard to the **NHC(II)**-catalyzed system, we optimized the two transition states involved in the enantioselectivity-determining (denoted as **TS21**(R/S)$_B$′ respectively, Figure 6). The calculated results reveal that the energy of **TS21**R_B′ is 3.0 kcal/mol lower than that of **TS21**S_B′, which is consistent with the experimental results.

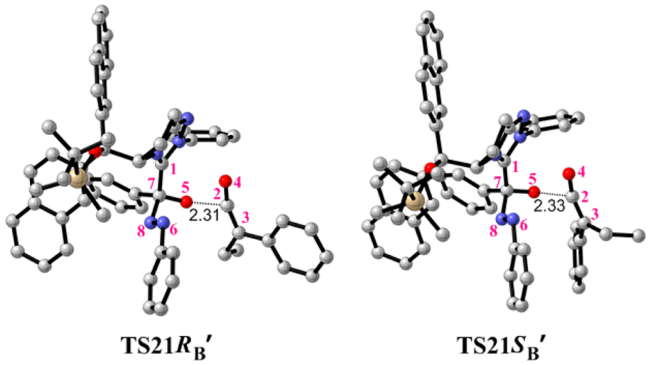

Figure 6. Optimized geometries of **TS21**R_B′ and **TS21**S_B′ (all hydrogen atoms are omitted; units in angstroms for bond lengths).

4. CONCLUSIONS

The DFT calculations carried out in this work have afforded the detailed computational study on possible mechanisms and enantioselectivity for the title catalyzed [4 + 2] cycloaddition reaction. The calculated results demonstrate that the novel "diazene-first" mechanism B is more favorable than the "ketene-first" mechanism A since its lower energy barrier and rational explanations to the enantioselectivities along with the general experimental procedure. There are four steps in mechanism B, including first the nucleophilic attack of NHC to **R2**, then the following stepwise [4 + 2] cycloaddition and finally recovering of the catalyst. The enantioselectivity-determining step appears in the first process of cycloaddition, and the product of *S* configuration will be the major enantiomer when catalyzed by **NHC(I)**, whereas the *R* configuration will be major when catalyzed by **NHC(II)**. This is in good agreement with the experimental ee values and further proves the reliability of mechanism B.

The novel mechanistic insights obtained in this study should also be valuable for design of more efficient NHC catalysts and/or reactions to achieve diverse 1,3,4-oxadiazin-6-one heterocycle products with desired optical activities.

dx.doi.org/10.1021/jo302044n | *J. Org. Chem.* 2012, 77, 10729−10737

■ ASSOCIATED CONTENT

Supporting Information

List of Cartesian coordinates, absolute electronic energies (E) and Gibbs free energies (G) (in hartrees, Table S1) of all stationary points involved in this study. Test results of M05-2X calculations at the 6-31G* level (Figure S1). Free energy profiles of mechanisms A and B (Figure S2). Comparisons of relative energies of B3LYP/6-311+G** optimization with single-point refinement for selected stationary points (Table S2). This material is available free of charge via the Internet at http://pubs.acs.org/.

■ AUTHOR INFORMATION

Corresponding Author

*E-mail: zhuyan@zzu.edu.cn, mstang@zzu.edu.cn.

Notes

The authors declare no competing financial interest.

■ ACKNOWLEDGMENTS

The work described in this paper was supported by the National Natural Science Foundation of China (No. 21001095), China Postdoctorial Science Foundation (No. 20100480858), and Excellent Doctoral Dissertation Engagement Fund of Zhengzhou University in 2012.

■ REFERENCES

(1) (a) Tidwell, T. T. Reactions of Ketenes. *Ketenes II*, 2nd ed.; John Wiley & Sons, Inc.: Hoboken, NJ, 2006. (b) Tidwell, T. T. *Angew. Chem.* **2005**, *117*, 5926−5933. (c) Tidwell, T. T. *Angew. Chem., Int. Ed.* **2005**, *44*, 5778−5785. (d) Tidwell, T. T. *Eur. J. Org. Chem.* **2006**, *2006*, 563−576. (e) Orr, R. K.; Calter, M. A. *Tetrahedron* **2003**, *59*, 3545−3565.

(2) Glorius, F.; Hirano, K., Nucleophilic Carbenes as Organocatalysts. *Ernst Schering Foundation Symposium Proceedings*; Springer-Verlag: Berlin, 2008; Vol. 2, pp 159−181.

(3) Enders, D.; Balensiefer, T. *Acc. Chem. Res.* **2004**, *37*, 534−541.

(4) Schrader, W.; Handayani, P. P.; Burstein, C.; Glorius, F. *Chem. Commun.* **2007**, 716−718.

(5) Zeitler, K. *Angew. Chem., Int. Ed.* **2005**, *44*, 7506−7510.

(6) (a) Wöhler, F.; Liebig, J. *Ann Pharm* **1832**, *3*, 249−282. (b) Enders, D.; Kallfass, U. *Angew. Chem., Int. Ed.* **2002**, *41*, 1743−1745. (c) Hachisu, Y.; Bode, J. W.; Suzuki, K. *J. Am. Chem. Soc.* **2003**, *125*, 8432−8433.

(7) Christmann, M. *Angew. Chem., Int. Ed.* **2005**, *44*, 2632−2634.

(8) (a) Zhang, Y. R.; He, L.; Wu, X.; Shao, P. L.; Ye, S. *Org. Lett.* **2008**, *10*, 277−280. (b) Duguet, N.; Campbell, C. D.; Slawin, A. M. Z.; Smith, A. D. *Org. Biomol. Chem.* **2008**, *6*, 1108−1113.

(9) He, L.; Lv, H.; Zhang, Y.-R.; Ye, S. *J. Org. Chem.* **2008**, *73*, 8101−8103.

(10) Wang, X.-N.; Shen, L.-T.; Ye, S. *Chem. Commun.* **2011**, *47*, 8388−8390.

(11) Zhang, Y.-R.; Lv, H.; Zhou, D.; Ye, S. *Chem.—Eur. J.* **2008**, *14*, 8473−8476.

(12) Huang, X.-L.; He, L.; Shao, P.-L.; Ye, S. *Angew. Chem., Int. Ed.* **2009**, *48*, 192−195.

(13) (a) Markert, J.; Fahr, E. *Tetrahedron Lett.* **1970**, *11*, 769−772. (b) Kerber, B. C.; Ryan, T. J.; Hsu, S. D. *J. Org. Chem.* **1974**, *39*, 1215−1221.

(14) (a) El-Shenawy, A. I.; Aly, A. A. *Egypt. J. Chem* **2005**, *48*, 781−788. (b) Pfeiffer, W.-D., *Comprehensive Heterocyclic Chemistry III*; Katritzky, A., Ramsden, C., Scriven, E., Taylor, R., Eds.; Elsevier Science: Dordrecht, Vol. 9, 2008; pp 401−455.

(15) (a) Freeman, J. P.; Surbey, D. L.; Kassner, J. E. *Tetrahedron Lett.* **1970**, *11*, 3797−3780. (b) Farina, C.; Pifferi, G.; Nasi, F.; Pinza, M. *J. Heterocycl. Chem.* **1983**, *20*, 979−982. (c) Taylor, E. C.; Clemens, R. J.; Davies, H. M. L.; Haley, N. F. *J. Am. Chem. Soc.* **1981**, *103*, 7659−7660. (d) Taylor, E. C.; Davies, H. M. L.; Clements, R. J.; Yanagisawa, H.; Haley, N. F. *J. Am. Chem. Soc.* **1981**, *103*, 7660−7661. (e) Taylor, E. C.; Davies, H. M. L.; Lavell, W. T. *J. Org. Chem.* **1984**, *49*, 2204−2208.

(16) (a) Cativiela, C.; Díaz-de-Villegas, M. D. *Tetrahedron: Asymmetry* **2007**, *18*, 569−623. (b) Vogt, H.; Bräse, S. *Org. Biomol. Chem.* **2007**, *5*, 406−430.

(17) Tang, K.; Wang, J. H.; Cheng, X. L.; Hou, Q. Q.; Liu, Y. J. *Eur. J. Org. Chem.* **2010**, 6249−6255.

(18) Wei, D. H.; Zhu, Y. Y.; Zhang, C.; Sun, D. Z.; Zhang, W. J.; Tang, M. S. *J. Mol. Catal. A: Chem.* **2011**, *334*, 108−115.

(19) (a) Parr, R. G.; Pearson, R. G. *J. Am. Chem. Soc.* **1983**, *105*, 7512−7516. (b) Domingo, L. R.; Saéz, J. A.; Zaragozá, R. J.; Arnó, M. *J. Org. Chem.* **2008**, *73*, 8791−8799. (c) Domingo, L. R.; Aurell, M. J.; Pérez, P.; Contreras, R. *Tetrahedron* **2002**, *58*, 4417−4423. (d) Domingo, L. R.; Sáez, J. A. *Org. Biomol. Chem.* **2009**, *7*, 3576−3583. (e) Domingo, L. R.; Picher, M. T.; Sáez, J. A. *J. Org. Chem.* **2009**, *74*, 2726−2735. (f) Kohn, W.; Sham, L. *J. Phys. Rev.* **1965**, *140*, 1133−1138. (g) Domingo, L. R.; Chamorro, E.; Perez, P. *J. Phys. Chem. A* **2008**, *112*, 4046−4053. (h) Domingo, L. R.; Chamorro, E.; Perez, P. *J. Org. Chem.* **2008**, *73*, 4615−4624.

(20) (a) Jørgensen, K. A. *Angew. Chem.* **2000**, *112*, 3702−3733. (b) Jørgensen, K. A. *Angew. Chem., Int. Ed.* **2000**, *39*, 3558−3588. (c) Waldmann, H. *Synlett* **1995**, 133−141. (d) Tietze, L. F.; Kettschau, G. *Top. Curr. Chem.* **1997**, *189*, 1−120. (e) Weinreb, S. M. *Top. Curr. Chem.* **1997**, *190*, 131−184. (f) Kobayashi, S.; Ishitani, H. *Chem. Rev.* **1999**, *99*, 1069−1094.

(21) (a) Bailey, R. T.; Garigipati, R. S.; Morton, J. A.; M.Weinreb, S. *J. Am. Chem. Soc.* **1984**, *106*, 3240−3245. (b) Lock, R.; Waldmann, H. *Liebigs Ann. Chem.* **1994**, 511−516. (c) Holmes, A. B.; Kee, A.; Ladduwahetty, T.; Smith, D. F. *J. Chem. Soc., Chem. Commun.* **1990**, 1412−1414.

(22) In fact, only the experimental procedure catalyzed by **NHC(II′)** (Ar^1 = Ar^2 = Ph, R = OTBS, Scheme 1) is available from ref 12. But we believe it is also applicable to other reactions characterized as a similar category and reported in the same work without any special statements. Besides, it has not been chosen as our computational model because the reaction yield and ee values catalyzed by **NHC(II′)** are both lower than that by **NHC(II)**.

(23) Frisch, M. J.; Trucks, G. W.; Schlegel, H. B.; Scuseria, G. E.; Robb, M. A.; Cheeseman, J. R.; Scalmani, G.; Barone, V.; Mennucci, B.; Petersson, G. A.; Nakatsuji, H.; Caricato, M.; Li, X.; Hratchian, H. P.; Izmaylov, A. F.; Bloino, J.; Zheng, G.; Sonnenberg, J. L.; Hada, M.; Ehara, M.; Toyota, K.; Fukuda, R.; Hasegawa, J.; Ishida, M.; Nakajima, T.; Honda, Y.; Kitao, O.; Nakai, H.; Vreven, T.; Montgomery, J. A., Jr.; Peralta, J. E.; Ogliaro, F.; Bearpark, M.; Heyd, J. J.; Brothers, E.; Kudin, K. N.; Staroverov, V. N.; Keith, T.; Kobayashi, R.; Normand, J.; Raghavachari, K.; Rendell, A.; Burant, J. C.; Iyengar, S. S.; Tomasi, J.; Cossi, M.; Rega, N.; Millam, J. M.; Klene, M.; Knox, J. E.; Cross, J. B.; Bakken, V.; Adamo, C.; Jaramillo, J.; Gomperts, R.; Stratmann, R. E.; Yazyev, O.; Austin, A. J.; Cammi, R.; Pomelli, C.; Ochterski, J. W.; Martin, R. L.; Morokuma, K.; Zakrzewski, V. G.; Voth, G. A.; Salvador, P.; Dannenberg, J. J.; Dapprich, S.; Daniels, A. D.; Farkas, O.; Foresman, J. B.; Ortiz, J. V.; Cioslowski, J.; Fox, D. J. Gaussian 09, Revision C. 01; Gaussian, Inc.: Wallingford, CT, 2010.

(24) (a) Zhang, C.; Zhu, Y. Y.; Wei, D. H.; Sun, D. Z.; Zhang, W. J.; Tang, M. S. *J. Phys. Chem. A* **2010**, *114*, 2913−2919. (b) Domingo, L. R.; Pérez-Ruiz, R.; Argüello, J. E.; Miranda, M. A. *J. Phys. Chem. A* **2009**, *113*, 5718−5722.

(25) Gonzalez, C.; Schlegel, H. B. *J. Chem. Phys.* **1989**, *90*, 2154−2161.

(26) Gonzalez, C.; Schlegel, H. B. *J. Phys. Chem. A* **1990**, *94*, 5523−5527.

(27) (a) Sang-Aroon, W.; Ruangpornvisuti, V. *Int. J. Quantum Chem.* **2008**, *108*, 1181−1188. (b) Tomasi, J.; Mennucci, B.; Cancès, E. *THEOCHEM* **1999**, *464*, 211−226.

(28) (a) Reed, A. E.; Weinhold, F. *J. Chem. Phys.* **1983**, *78*, 4066−4073. (b) Foster, J. P.; Weinhold, F. *J. Am. Chem. Soc.* **1980**, *102*,

7211−7218. (c) Glendening, E. D.; Reed, A. E.; Carpenter, J. E.; Weinhold, F. NBO Version 3.1.
(29) Huang, F.; Zhang, C. G.; Jiang, J. L.; Wang, Z.-X.; Guan, H. R. *Inorg. Chem.* **2011**, *50*, 3816−3825.
(30) Lan, Y.; Houk, K. N. *J. Org. Chem.* **2011**, *76*, 4905−4909.
(31) (a) Starr, C.; Evers, C. A.; Starr, L. *Biology: Concepts and Applications*; Thomson Brooks/Cole: Pacific Grove, CA, 2006. (b) Nye, M. J. *The Cambridge History of Science: The Modern Physical and Mathematical Sciences*; Cambridge University Press: Cambridge, 2003; Vol. *5*, p 278. (c) Brand, J. C. D., *Lines of Light: The Sources of Dispersive Spectroscopy. 1800−1930*; CRC Press: Boca Raton, 1995; p 30.